Journal of Imaging Science and Technology® 50(6): 522–529, 2006.

Banding Assessment with Controlled Halftoning: The Ten Printer Experiment

Yousun Bang▲,†
School of Electrical and Computer Engineering, Purdue University, West Lafayette, Indiana 47907
E-mail: ybang@ecn.purdue.edu

Zygmunt Pizlo
Department of Psychological Sciences, Purdue University, West Lafayette, Indiana 47907

Jan P. Allebach▲
School of Electrical and Computer Engineering, Purdue University, West Lafayette, Indiana 47907

Abstract. *Printer banding which appears as nonuniform light and dark lines across a printed page have been an important image quality issue in the printing industry, and have been studied by many researchers. However, no literature has reported banding perception in different printers with different characteristics of banding. In this paper the authors develop a tool for measuring banding based on human perception. The authors describe new cross-platform experiments using ten different laser printers having different imaging characteristics. In order to focus on the impact of the printer mechanism on banding and to remove the confounding effect of the halftoning algorithm, the authors employ a specially designed line screen with all the test printers. The authors use the pulse width modulation capability of a single reference printer to match the absorptance of these printers, and to also generate extrinsic banding signals. The experimental results identify the points of subjective equality of the ten printers relative to the banding of a reference printer, and provide the basis of a method of computing banding power by considering a contrast sensitivity function. The authors results show that regardless of the different banding spectral characteristics, the contrast banding power of a given printer can be mapped to a perceptually equivalent level of contrast banding power of one reference printer with added extrinsic banding. © 2006 Society for Imaging Science and Technology.*
[DOI: 10.2352/J.ImagingSci.Technol.(2006)50:6(522)]

INTRODUCTION

Banding usually appears as nonuniform light and dark lines across a printed page perpendicular to the direction in which the paper passes through the printer. Banding is primarily caused by quasiperiodic fluctuations in the parameters of the print mechanism; but it is strongly influenced by the algorithms in the imaging pipeline as well—especially the halftoning process. Banding is an important image quality topic in the printing industry. Many researchers have tried to find answers to the following questions: First, what causes printer banding?[1–4] Second, how can banding be measured or modeled?[5–9] Third, how visible is banding to observers?[10–13] Finally, how do we reduce banding?[14–16] In the above four categories of banding study, a considerable amount of work has been reported. However, no simple answers have yet been found.

A major source of difficulty is the fact that different printers have very different characteristics of banding. Depending on printer engines, printing systems, or product model numbers, the amount of banding and the frequencies of banding are quite different. The question is how we can obtain a general banding metric which can apply for all printer models. Since banding is a perceptual phenomenon as well as a physical phenomenon, we also incorporate the human visual system in developing a banding metric. Once we have the metric, it will provide a very helpful guide in designing a new printer with reduced banding.

So far no literature has reported comparison results of banding levels in different printers. In this paper, we design a novel cross-platform experiment using as test printers ten different monochrome laser printers having different banding spectral contents, compare the levels of banding with a single reference printer, and then establish a banding metric which reliably predicts the level of banding in the reference printer that will be judged to be a match to the test printer. In their previous work,[12] the authors described a methodology for measuring an observer's ability to discriminate between images having different levels of banding for a given printer. To control banding levels, an α level of extrinsic banding was added to the printer intrinsic banding. We will employ a similar methodology to measure the visibility of banding across different printers. However, comparing the banding levels of different printers involves two important considerations.

First, we must take into account the influence of the halftone patterns of different printers. Each printer has its own halftone patterns; and it is well known that screen angles, screen frequencies, or dot arrangements are strongly correlated to the visibility of banding. In this study, we are only interested in the impact of the printer mechanism on

▲IS&T Member.
†Corresponding author. Present address: Samsung Advanced Institute of Technology, San 14-1, Nongseo-Dong, Giheung-Gu, Yongin-Si, Gyeonggi-Do, South Korea.

Received Jan. 9, 2006; accepted for publication Aug. 15, 2006.
1062-3701/2006/50(6)/522/8/$20.00.

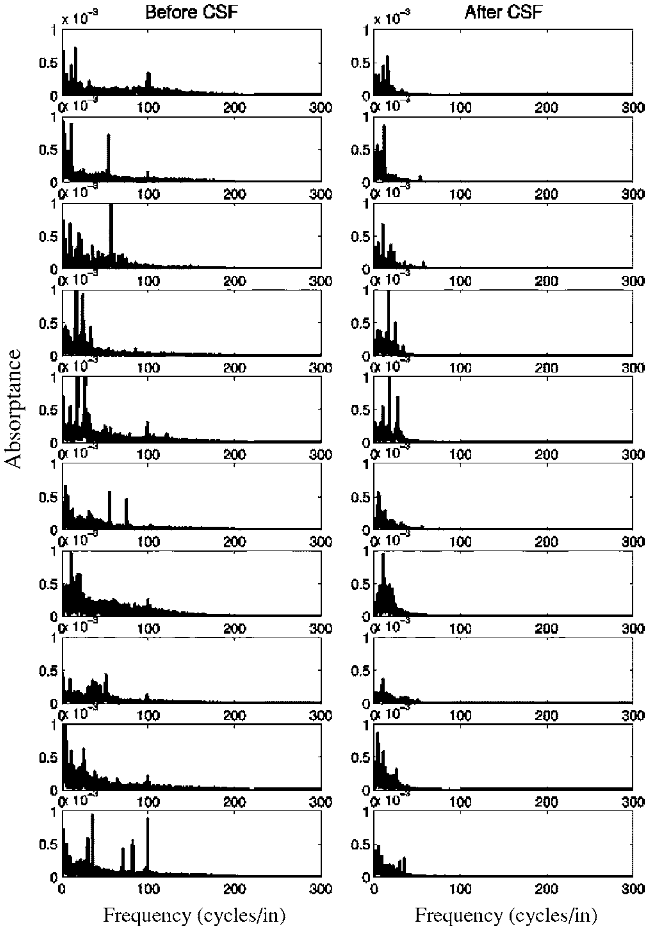

Figure 1. Spectral plots of the ten test printers before and after applying contrast sensitivity function for a viewing distance of 45 in.

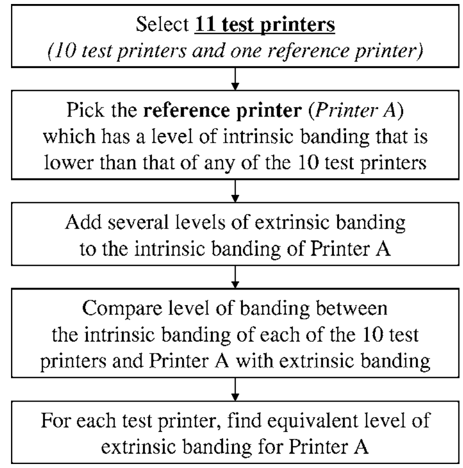

Figure 2. Our approach to the study of banding assessment.

banding. Therefore, we should control the effect of halftone patterns by applying the same pattern to all ten of the printers. We also use a very simple halftone pattern—a vertical line pattern—that has a consistent structure across the entire tone scale. This further reduces the impact of the halftoning on our investigation of banding.

Second, we also need to consider the tone dependency of banding visibility. Thus, we should properly calibrate the printers to compare images with the same tone levels. In this paper, we use the pulse width modulation capability of the reference printer to solve this problem.

The rest of the paper is organized as follows. In the next section, we describe our framework for the ten-printer experiment, and show how we generate image samples. Then we present the procedures for the psychophysical cross-platform experiments. Finally, we discuss our experimental results and draw some conclusions.

GENERAL FRAMEWORK OF THE TEN-PRINTER EXPERIMENT

To obtain a reliable banding metric, we design psychophysical experiments using 11 different printers with different spectral contents. Among the 11 printers, one is chosen as a reference printer, and the others serve as test printers. Regarding the test printers, ten monochrome laser printers having various levels of intrinsic banding were carefully chosen for our experiments: They are made by six different manufacturers, and range from very low-end to high-end market segments for monochrome laser printers. The left column in Fig. 1 shows banding spectra of these ten test printers. As seen in the figure, these ten printers have very different spectral characteristics. The peaks in the banding spectra are located in different places, which means that amplitudes and frequencies of banding are different from printer to printer. Our aim is to measure the perceived amount of intrinsic banding of the test printers by identifying the equivalent amounts of extrinsic banding for the reference printer. Thus, for the reference printer, we picked a printer which showed a lower level of banding than each of the ten test printers. Then we could add extrinsic banding to the intrinsic banding of the reference printer for the comparison with each of the test printers. In this paper, we will call this reference printer *Printer A*. Our approach is summarized in the block diagram in Fig. 2.

When we measure visibility of banding with different printers, we want to avoid having the role of the halftoning algorithm influence our results. We will show how we designed the patches for our experiments to achieve this objective.

PATCH DESIGN WITH LINE PATTERNS

We design a special patch consisting of lines parallel to the paper process direction. Since banding occurs in the direction perpendicular to the paper process direction, we do not want the line patterns to influence banding visibility. With each of the ten test printers, we use the same $[0,1,1,0,0]$ repeated line pattern, where 0 is white, and 1 is black. This is illustrated in Fig. 3 where the zoomed area shows four repeated $[0,1,1,0,0]$ line patterns.

When we print this patch using the ten printers, each printed patch appears uniform gray at a 12 in. normal viewing distance, ignoring banding and other potential artifacts. We measured the luminance CIE Y values of the ten patches

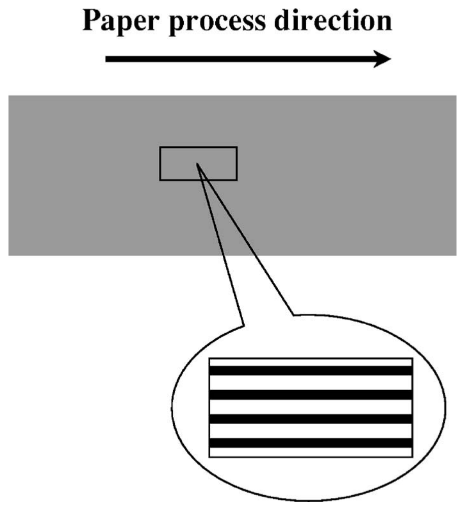

Figure 3. Test patch having the 01100 line pattern.

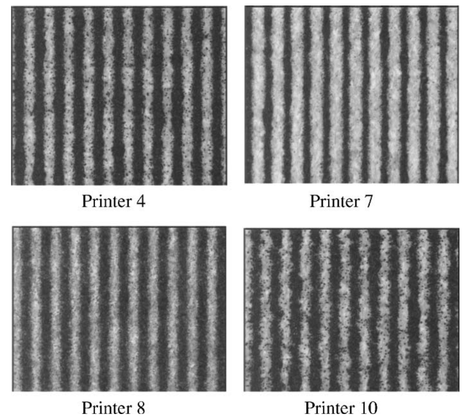

Figure 4. Test patches with the 01100 line pattern for four test printers, scanned at 7100 dpi.

Table I. Average luminance Y of $[0,1,1,0,0]$ and tone-matched base line pattern of Printer A.

Test printer	Average Y luminance	Base line pattern
Printer 1	29.28	[1 63 63 1 0]
Printer 2	22.18	[21 63 63 21 0]
Printer 3	22.24	[21 63 63 21 0]
Printer 4	22.69	[21 63 63 21 0]
Printer 5	26.56	[8 63 63 8 0]
Printer 6	30.77	[0 54 54 0 0]
Printer 7	37.82	[0 38 38 0 0]
Printer 8	24.30	[15 63 63 15 0]
Printer 9	24.51	[15 63 63 15 0]
Printer 10	22.03	[21 63 63 21 0]

with a spectrophotometer (Gretag SPM 50: Gretag AG, Zürich, Switzerland). The options of "absolute white," "D65 light," and "no filter" were selected to calibrate a white point using the "SPM 50 standard target." The measured luminance Y values vary from 22.03 to 37.82 in units of absorptance as shown in Table I. Figure 4 shows the scanned test patches having the 01100 line patterns for four test printers. Here, they were scanned at the resolution of 7100 dpi using a print quality evaluation system (QEA IAS-1000: Quality Engineering Associates, Inc., Burlington, MA). As shown, test prints with the same [01100] pattern have different absorptance values.

In the following sections, we will describe how we matched the absorptance between Printer A and each test printer, and also show how to generate the extrinsic banding signal for each test printer.

Table II. Justification modes used for our reference patch design.

Pulse width code	Pulse justification code (right, left, center)
$[0,x,x,0,0]$	$[-,R,L,-,-]$
$[y,63,63,y,0]$	$[R,C,C,L,-]$

REFERENCE PATCH DESIGN AND CALIBRATION OF LINE PATTERNS

Because of the tone dependency of banding visibility, we should match the absorptance when comparing the banding levels of two different printers. By using the pulse width modulation (PWM) capability of Printer A, we vary the tone of Printer A to match the absorptance of the test printer that is obtained when we print the fixed 01100 pattern. Printer A accepts an 8 bit PWM code for each pixel. Six bits control the pulse width and two bits determine the pulse justification. With this, each pixel can have 64 gray levels from 0 (white) to 63 (black), and can be left, center, right, or split justified.

For an exact tone match, we need to perform a calibration process of Printer A with the line patterns. To do this, we designed 1273 in. $\times 7$ in. gray patches having repeated line patterns of the form $[0,x,x,0,0]$ or $[y,63,63,y,0]$, where x and y are gray values between 0 and 63. In order to make the PWM printing more stable, we used the justification codes shown in Table II. In the table, R, L, and C stand for right, left, and center justification, respectively. For convenience, we now represent our PWM codes by P, where

$$P = x, \quad \text{if line pattern is of the form of } [0,x,x,0,0]$$
$$= y + 63, \quad \text{if it is of the form of } [y,63,63,y,0]. \qquad (1)$$

We printed the reference patches at the default resolution of 600 dpi. We then measured the luminance Y values of the patches using the spectrophotometer. Since there were

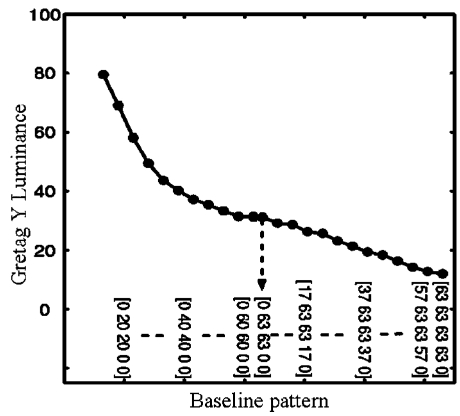

Figure 5. Measured Gretag *Y* luminance vs corresponding line patterns.

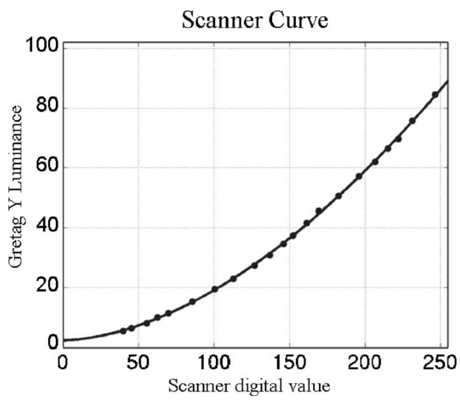

Figure 6. Scanner calibration curve measured by Gretag spectrophotometer.

small variations within each printed patch, we measured the values at five different locations along the patch and took the average value. The measured calibration curve is shown in Fig. 5. The plot shows that the measured Y values decrease smoothly as x and y increase from 0 to 63 in the line patterns of the form $[0,x,x,0,0]$ and $[y,63,63,y,0]$.

By applying the inverse of this calibration curve to the luminance Y value of the printed 01100 patch for each test printer, we obtain the corresponding line pattern which produces the same absorptance for Printer A. In this paper, we will call this tone-matched line pattern the base line pattern for the test printer. Table I shows the average Y values and the corresponding base line patterns of Printer A for the ten test printers. We then use reference patches with these line patterns for our banding experiments. For example, we use a reference patch with the $[1,63,63,1,0]$ base line pattern for the experiment between Printer 1 and Printer A, and a reference patch with the $[21,63,63,21,0]$ base line pattern for the experiment between Printer 2 and Printer A, and so on.

MODULATION PROCESS FOR EXTRINSIC BANDING

To generate various levels of extrinsic banding for Printer A, we extracted a one-dimensional prototype banding signal from each reference patch printed with the tone-matched

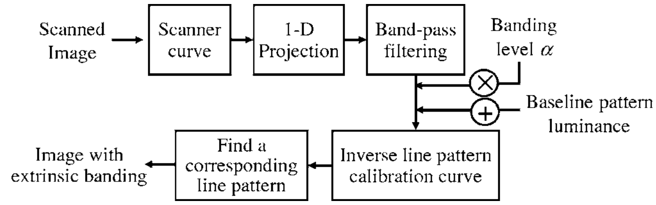

Figure 7. The procedure for generating digital image with extrinsic banding.

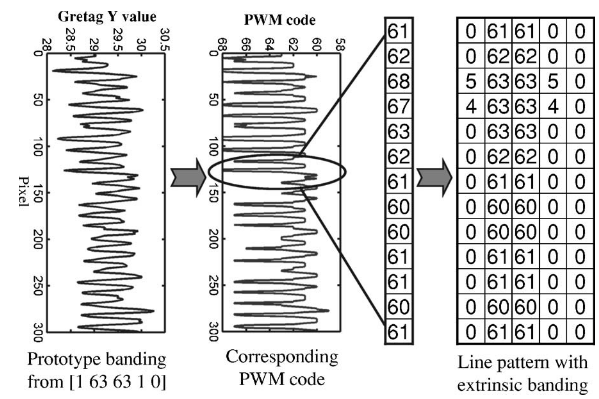

Figure 8. The modulation process for generating a reference patch with extrinsic banding.

line pattern using Printer A, and scanned using a flatbed scanner (Heidelberg Saphir Ultra2: Heidelberg USA, Inc., Kennesaw, GA 30144). To do this, we employed the method described in the paper by Bang et al.[12] We applied the scanner calibration curve shown in Fig. 6 to the scanned image, and then averaged the values in the direction perpendicular to the printer process direction to get a one-dimensional (1D) banding profile in units of Gretag Y luminance. We filtered the 1D banding signal in the spatial domain using a fifth order Butterworth bandpass filter with the cutoff frequencies 1 and 200 cycles/in. To prevent phase from affecting the results of experiments, we randomly shifted the phase of the extrinsic banding signal whenever we printed the image with extrinsic banding.

The entire procedure for generating a digital image with extrinsic banding is shown in Fig. 7. For each base line pattern, we multiplied the prototype banding signal by the banding level to obtain an α-level extrinsic banding signal. Here, α is the amount of extrinsic banding relative to the amount of intrinsic banding. The value $\alpha=0$ means no extrinsic banding is added; and $\alpha=1$ means that the amount of extrinsic banding added is the same as that of the intrinsic banding. Then we added the average luminance of the reference patch to the α-level extrinsic banding signal. Next, we applied a calibration curve which is the inverse of the curve shown in Fig. 5 to the α-level extrinsic banding signal, and found a corresponding line pattern for each scan line. By concatenating those line patterns in the paper scan direction, we obtained the digital image with α-level extrinsic banding.

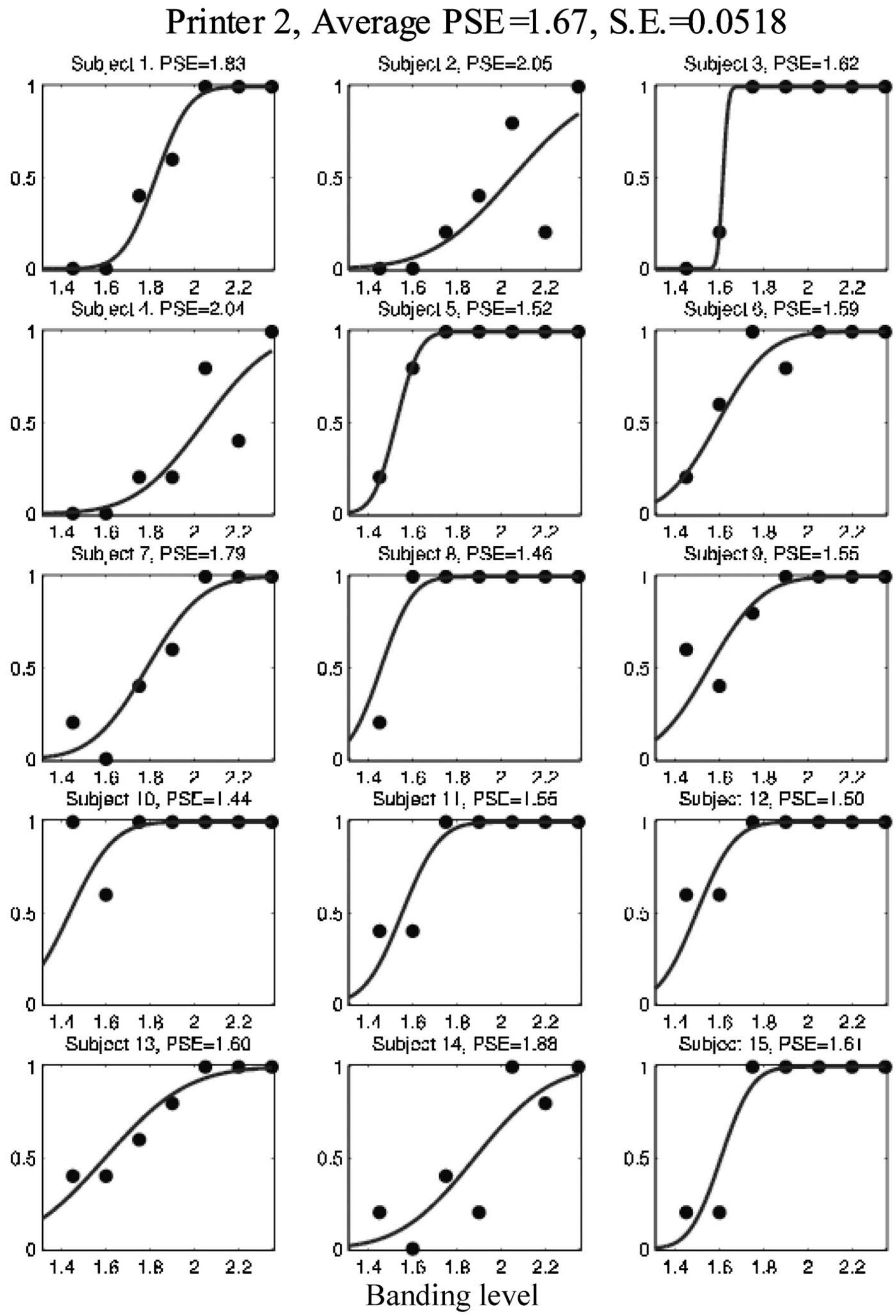

Figure 9. Estimated psychometric functions for Printer 2.

In Fig. 8, the modulation process of the line patterns is illustrated: For the base line pattern $[1,63,63,1,0]$, the prototype banding was extracted, and then converted into the PWM codes P. Then the PWM codes were expanded according to Eq. (1) to the corresponding line patterns in the direction perpendicular to the lines. The array on the far right side shows the image with an extrinsic banding signal. Therefore, for a given α we can generate an image with an extrinsic banding signal by using the pulse codes.

CROSS-PLATFORM EXPERIMENTS

For each of the ten test printers, we created print samples with both intrinsic and extrinsic banding using Printer A. We carefully selected the range of banding levels α for each test printer. Since all ten printers have different levels of banding, the ranges of α chosen varied from printer to printer as shown in the third column of Table III. We used the method of constant stimuli in our cross-platform experiments. For each session, image stimuli with eight levels of α were used. Using five different prints for each banding level, each subject did a total of 40 trials for each session. In the method of constant stimuli, on each trial the print sample from the test printer and various levels of reference stimuli from Printer A were presented to the subject. The test print contained only intrinsic banding of the test printer, and the reference prints contained intrinsic plus extrinsic banding of Printer A. The level of the reference stimulus varied randomly from trial to trial.

We used mat boards (MatShop/Island Art Shop: Bellingham, WA 98226) for our experiments and mounted all the prints on the boards. We used the regular mat with neutral color Crescent 934 Pearl for the core (outer mat size: 10 in. × 13 in., opening size: 7.5 in. × 10 in) and white regular mat for backing. We labeled the mounted prints with a randomly generated integer.

We conducted the experiments in a normal office environment. For each test printer, 13–15 Purdue graduate students participated in our experiments. The subject's task was to say whether the reference image had more or less banding than the test print. For each trial, the subjects were allowed to take as long as they wished to make a decision. Each subject took about 30 min to complete the experiment with the 40 stimuli. They recorded their answers on a computer. By analyzing the subjects' responses, we computed the probabilities that the subjects discriminated between the test print and the reference stimuli, and estimated psychometric functions of the subjects. Since a perceptual Gaussian model is widely accepted in psychophysics, we conducted a Probit analysis to fit a normal cumulative function to our data.[17] We then obtained an equivalent banding level of Printer A for each test printer. This equivalent level is called the point of subjective equality (PSE), and each subject's PSE can be estimated by the mean value of the fitted cumulative Gaussian function. In the next section, we will present our experimental results.

RESULTS AND DISCUSSION

For each of the ten test printers, we obtained psychometric functions for each subject by conducting a series of Probit analyses. Figure 9 shows the estimated psychometric functions for Printer 2. They are generally well fitted by Gaussian functions.

We computed the average PSE and the standard error for each test printer. The standard error is the estimated standard deviation of the average PSE. The measured average PSE for each test printer is the banding level of Printer A at which an average subject judges that the intrinsic banding of the test printer is perceptually equivalent to that of the reference printer. Table III shows the average PSE obtained for each test printer. Among the ten printers, Printer 9 had the lowest PSE, and Printer 7 had the highest PSE, which was greater by a factor of 5. This shows that the visibility of banding varies substantially from printer to printer.

Regardless of the different spectral contents, the subjects successfully performed the experiments; and they were all able to compare the banding levels of the two different printers during each trial. After obtaining the PSE's for the ten printers, we generated the patches for Printer A with the extrinsic banding signals of those PSE levels. We printed them using Printer A; and based on informal visual comparisons we confirmed that they had a level of banding that is perceptually equivalent to the intrinsic banding of the test printers.

Table III. Average PSE with standard error and banding levels used.

Test printer	Average PSE	α levels used
Printer 1	1.53 (±0.053)	0.60–2.70
Printer 2	1.67 (±0.052)	1.30–2.35
Printer 3	0.81 (±0.027)	0.50–1.20
Printer 4	1.23 (±0.055)	0.90–1.81
Printer 5	1.05 (±0.056)	0.60–1.65
Printer 6	0.65 (±0.035)	0.30–1.00
Printer 7	2.54 (±0.083)	2.00–3.40
Printer 8	0.80 (±0.045)	0.50–1.41
Printer 9	0.51 (±0.066)	0.24–1.36
Printer 10	1.30 (±0.079)	0.75–1.80

BANDING METRIC

In order to establish a banding metric, we measured and compared the banding power of the intrinsic banding of the ten test printers and Printer A with the obtained PSE's. The method of computing banding power is described in the authors' previous work.[12] Using a periodogram method, we estimated the power spectral density of the bandpass filtered signal, and computed the average banding power. We normalized the banding power of the test printers by the reflectance squared to obtain the contrast banding power. Since banding perception depends on the contrast and spatial frequency content of the banding image, we applied Campbell's contrast sensitivity function (CSF) to the banding spectra. Figure 10 shows Campbell's CSF at a 12 in. viewing distance.

The banding signals associated with laser EP printers have a complex structure that varies significantly among different printer models. This can be seen in the left column of Fig. 1 which shows spectral plots for the ten printers that we investigated in this paper. In general, the banding spectra consist of one or more strong, distinct spectral lines against a broadband background of continuous spectral power. The distinct spectral lines are perceived as perfectly periodic bands superimposed on top of an irregular pattern that varies only in the process direction. In our earlier work, we found that for a single printer, the banding visibility scaled linearly with the power of the banding signal, integrated over a broad passband.[12] However, for the data obtained from the ten printers, we found that this was no longer the case. In particular, banding signals with strong, isolated high frequency components were less visible than would be predicted on the basis of their integrated spectral power, or the spectral power computed after normalizing the banding signal by the average gray value to yield contrast, and multiplying the banding spectrum by the HVS contrast sensitivity function for a normal viewing distance.

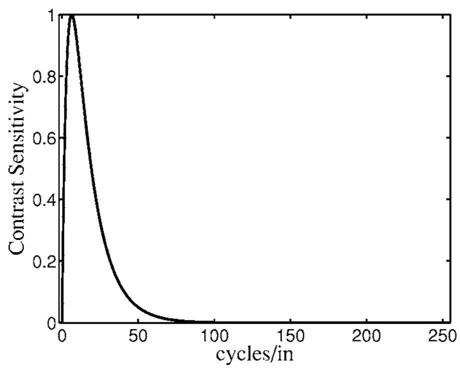

Figure 10. Campbell's contrast sensitivity function at a 12 in. viewing distance.

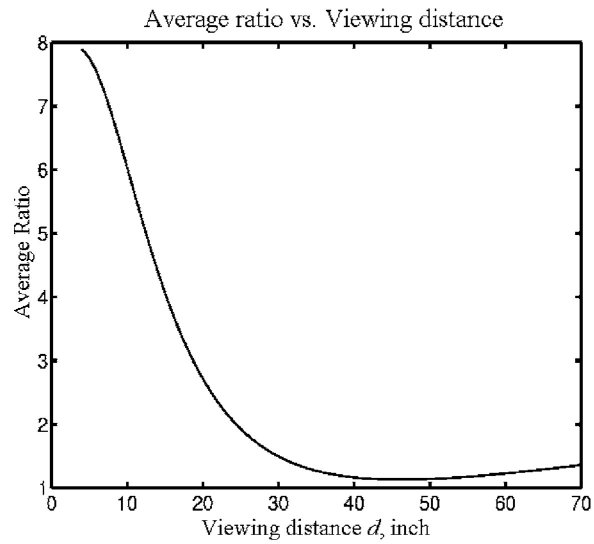

Figure 11. Mean-squared difference between the ratio of the contrast power of Printer A at the PSE to that of each of the ten test printers and unity as a function of the viewing distance d.

We hypothesized that the viewers were "seeing through" the strongly periodic high frequency component and thereby discounting it to some extent. This behavior would be consistent with the adaptive nature of the human visual system and the anecdotal evidence that viewers can easily see through a periodic, clustered-dot halftone texture to identify image detail, even when the halftone texture is actually quite visible. As just one possible way to account for this, we investigated the concept of increasing the effective viewing distance associated with the contrast sensitivity function, thereby attenuating the high frequency components. We view the PSEs determined by our psychophysical experiments as the true measure of relative banding visibility among the ten printers. Thus, we defined the cost function given in Eq. (2) as a measure of how well the visually weighted banding contrast power predicts PSE

$$\Phi(d) = \sum_{i=1}^{10} \left(\frac{P^d_{A+\mathrm{PSE}_i}/r^2_{A+\mathrm{PSE}_i}}{P^d_{\mathrm{test}_i}/r^2_{\mathrm{test}_i}} - 1 \right)^2 . \qquad (2)$$

Here, i is the index corresponding to the test printer, P^d is banding power after applying the CSF at a viewing distance d, r is the average reflectance of the patch, and the subscripts $A+\mathrm{PSE}_i$ and test_i stand for Printer A at the PSE for Printer i, and the ith test printer, respectively. This cost is a function of the viewing distance d. It is shown in Fig. 11. As can be seen there, 45 in. is the minimizing value for d. Therefore, we applied the CSF with a 45 in. viewing distance to the banding spectra of the test printers. Figure 1 shows the spectra of the ten test printers before and after applying the contrast sensitivity function at the 45 in. viewing distance.

Figure 12 shows the logarithm of the visually weighted contrast power for Printer A at the PSE versus the logarithm of the visually weighted contrast power for the test printer viewed at a distance of 45 in. The plot shows that for each test printer there is a strong correlation between the log contrast power of Printer A at the PSE for the test printer and the log contrast power of the test printer. Although the ten test printers have different spectral characteristics, the measured contrast power of intrinsic banding in the test printers can be mapped into the visually equivalent contrast power of Printer A. Therefore, this implies that we can quantify the perceived banding in a given printer by measuring the corresponding contrast power of one specific printer—Printer A.

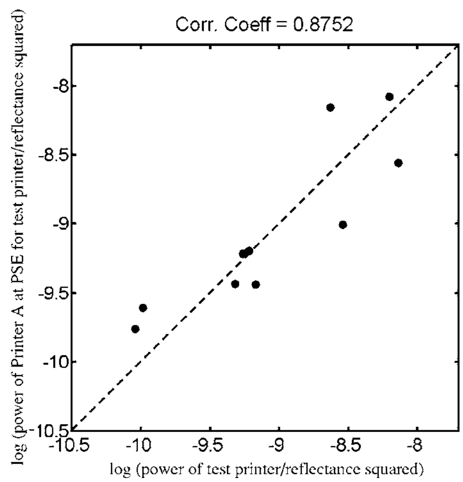

Figure 12. Log contrast power of Printer A at the PSE vs log contrast power of the ten test printers viewed at a distance of 45 in.

CONCLUSION

In the paper, we developed a novel methodology to compare the banding levels of different printers. We quantified the perceived banding of ten different printers by measuring the logarithmic contrast banding power. Based on our ten-printer experiment, we found that regardless of the different banding spectral contents, the contrast banding power of a given printer can be directly mapped to the contrast banding power of one reference printer with added extrinsic banding.

This suggests that we can reliably estimate the level of perceived banding in any laser printer, and thus our method can assist in the design of a new printer having reduced banding.

Acknowledgments

The authors gratefully acknowledge the support from the Hewlett Packard Company for this research; and would like to express sincere gratitude to Kainlu Low for his assistance during this project. They also wish to thank all the subjects who participated in the experiments.

REFERENCES

[1] D. D. Hass, "Contrast modulation in halftone images produced by vibration in scanline spacing," J. Imaging Technol. **15**, 46–55 (1989).

[2] R. Loce and W. Lama, "Halftone banding due to vibrations in a xerographic image bar printer," J. Imaging Technol. **16**, 6–11 (1990).

[3] R. P. Loce, W. L. Lama, and M. S. Maltz, "Modeling vibration-induced halftone banding in a xerographic laser printer," J. Electron. Imaging **4**, 48–61 (1995).

[4] J. H. You, H.-G. Kim, and S.-Y. Han, "Banding reduction in electrophotographic printer," in *Proc. IS&T's NIP20* (IS&T, Springfield, VA, 2004), pp. 470–473.

[5] Y. S. Ng, "Visual tolerance study with one-dimensional periodic (sinusoidal) and non-periodic (impulse) noise in electrophotographic gray level halftones," *Proc. IS&T's 11th International Congress on Advances in Non-Impact Printing Technologies* (IS&T, Springfield, VA, 1995), pp. 493–496.

[6] J. C. Briggs, M. Murphy, and Y. Pan, "Banding characterization for inkjet printing," *Proc. IS&T's PICS: Image Processing, Image Quality, Image Capture, Systems Conference* (IS&T, Springfield, VA, 2000) pp. 84–88.

[7] P. J. Kane, T. F. Bouk, P. D. Burns, and A. D. Thompson, "Quantification of banding, streaking and grain in flat field images," *Proc. IS&T's PICS: Image Processing, Image Quality, Image Capture, Systems Conference* (IS&T, Springfield, VA, 2000) pp. 79–83.

[8] D. R. Rasmussen, E. N. Dalal, and K. M. Natale-Hoffman, "Measurement of macrouniformity: Streaks, bands, mottle and chromatic variations," *Proc. IS&T's PICS: Image Processing, Image Quality, Image Capture, Systems Conference* (IS&T, Springfield, VA, 2001) pp. 90–95.

[9] W. Jang and J. P. Allebach, "Simulation of print quality defects," J. Imaging Sci. Technol. **49**, 1–18 (2005).

[10] C. Cui, D. Cao, and S. Love, "Measuring visual threshold of inkjet banding," *Proc. IS&T's PICS: Image Processing, Image Quality, Image Capture, Systems Conference* (IS&T, Springfield, VA, 2001) pp. 84–89.

[11] W. Wu, E. N. Dalal, and R. Rasmussen, "Perceptibility of non-sinusoidal bands," *Proc. IS&T's NIP18* (IS&T, Springfield, VA, 2002) pp. 462–466.

[12] Y. Bang, Z. Pizlo, and J. P. Allebach, "Discrimination based banding assessment," *Proc. IS&T's NIP19* (IS&T, Springfield, VA, 2003) pp. 745–750.

[13] O. Arslan, Z. Pizlo, and J. P. Allebach, "Softcopy banding visibility assessment," Proc. SPIE **5688**, 38–50 (2005).

[14] M. T. S. Ewe, J. M. Grice, G. T. C. Chiu, J. P. Allebach, C. S. Chan, and W. Foote, "Banding artifact reduction in electrophotographic processes using a piezoelectric actuated laser beam deflection device," J. Imaging Sci. Technol. **46**, 433–442 (2002).

[15] C. Chen and G. Chiu, "Banding reduction in electrophotographic process," *Proc. IEEE/ASME Int. Conf. Advanced Intelligent Mechatronics* (IEEE, Piscataway, NJ, 2001) pp. 81–86.

[16] G. Y. Lin, J. M. Grice, J. P. Allebach, G. T.-C. Chiu, W. Bradburn, J. Weaver, "Banding artifact reduction in electrophotographic printers by using pulse width modulation," J. Imaging Sci. Technol. **46**, 326–337 (2002).

[17] D. J. Finney, *Probit Analysis*, 3rd ed. (Cambridge University Press, Cambridge, UK, 1971).